PAPER

Dose coefficients for children and young adolescents exposed to external neutron fields

IOP Publishing | Society for Radiological Protection Journal of Radiological Protection
J. Radiol. Prot. **38** (2018) 587–606 (20pp) https://doi.org/10.1088/1361-6498/aab126

Dose coefficients for children and young adolescents exposed to external neutron fields

Keith Griffin, Matthew Mille and Choonsik Lee

Division of Cancer Epidemiology and Genetics, National Cancer Institute, National Institutes of Health, Rockville, MD 20850, United States of America

E-mail: choonsik.lee@nih.gov

Received 27 November 2017, revised 5 February 2018
Accepted for publication 21 February 2018
Published 28 March 2018

Abstract

The risks associated with exposure to external fields of ionising radiation are important to quantify in order to provide guidance towards public and worker protection. In Publication 116 of 2010, the International Commission on Radiological Protection (ICRP) published adult male and female fluence-to-dose coefficients (henceforth referred to as dose coefficients) for external exposures to six types of idealised neutron fields. However, ICRP 116 dose coefficients are not appropriate for applications involving children due to their smaller body weight and stature. Our current work details dose coefficient calculations for children and young adolescents using the UF-NCI pediatric hybrid phantoms at all neutron energies considered in ICRP 116 (0.001 eV to 10 GeV); those dose coefficients with energy up to 150 MeV are discussed. The hybrid UF-NCI phantoms are divided into five separate age groups: newborn, 1, 5, 10, and 15 years. For these phantoms, we calculated dose coefficients for the six idealised neutron fields for 28 organs, two bone tissues, and the overall whole body effective dose. All calculations were performed using the MCNP6 radiation transport code. To validate our methodology, we first calculated dose coefficients for the ICRP adult male and female phantoms and confirmed our ability to reproduce the values published within ICRP 116. The same methodology was then applied to calculate dose coefficients for the UF-NCI pediatric phantoms. Energy-dependent trends were observed in the neutron dose coefficients for pediatric phantoms: below 100 keV, dose increases with phantom age (a proxy for body size); however, above 100 keV, the opposite trend was observed. Comparisons between field geometries showed varying trends depending on the location of the organ within the body. Explanations for these trends are also explored within. Our results are the first comprehensive set of neutron dose coefficients derived for children and young

adolescents using the newest generation of hybrid phantoms. The primary application of the pediatric neutron dose coefficients presented in this work will be for a planned effort to update the dosimetry for the Japanese atomic bomb survivors.

Supplementary material for this article is available online

Keywords: external neutron, Monte Carlo radiation transport, organ dose, computational phantoms, children

(Some figures may appear in colour only in the online journal)

1. Introduction

The potential exposure of the nuclear workforce and members of the public to radioactive sources has driven the need for a convenient way to convert measurable quantities in the environment to estimates of health risk. In particular, the radiation epidemiologist aims to relate organ-absorbed dose to the incidence of subsequent cancer or other adverse health outcomes in a cohort of exposed individuals. However, the primary quantity of interest, organ absorbed dose, cannot be directly measured. Instead, one must convert a measurable quantity, such as particle fluence, to organ dose through the use of calculated fluence-to-dose conversion coefficients. The fluence-to-dose conversion coefficients (henceforth referred to as dose coefficients) can be calculated using computational human phantoms combined with Monte Carlo radiation transport simulation.

Computational human phantoms have evolved significantly since the first phantoms were developed in the 1960s [1]. The first generation of computational phantoms, often called stylised or mathematical phantoms, were defined using simple geometrical shapes and surfaces to represent each anatomical boundary. Though these mathematical phantoms offered great flexibility through their ability to easily rotate, reposition, and scale, they generally suffered from a lack of anatomical realism. Voxel phantoms, the second generation of computational phantoms, are defined as a three-dimensional matrix of pixels developed from segmented tomographic medical images. Though much more realistic than mathematical phantoms, voxel phantoms are fundamentally rigid; the body size and position of voxel phantoms cannot be easily modified or deformed to match the body type of a specific individual. These shortcomings resulted in the creation of the third and latest generation of phantoms, known as the hybrid phantoms, which are represented by a polygonal mesh. Hybrid phantoms capture the best qualities of previous phantom generations, anatomical realism and flexibility, and can be converted to a voxel phantom format as necessary for use in radiation transport codes.

For the purposes of standardization in the fields of radiation protection and dosimetry, the International Commission on Radiological Protection (ICRP) published an adult male and female reference voxel set in ICRP Publication 110 of 2009 [2]. A more recent publication, ICRP Publication 116, utilises these adult voxel phantoms to calculate and tabulate dose coefficients for external radiation exposures to idealised fields of multiple different particle types; particles such as photons, neutrons, and protons have dose coefficients tabulated for six different irradiation geometries meant to represent occupational exposure: antero-posterior (AP), postero-anterior (PA), left and right lateral (LLAT/RLAT), rotational (ROT), and isotropic (ISO) [3]. Though these dose coefficients have extensive applications, one clear

limitation is in their relevance only for reference-sized adults; children have too significant a difference in body weight and stature for appropriate application of dose coefficients derived for adults. Furthermore, the radiation exposure assessment of children and young adolescents can be truly important to consider, particularly in light of their long remaining life expectancy and increased radiosensitivity of their developing tissues [4].

Our current work aims to use the ICRP 116 methodology to calculate external dose coefficients for children and young adolescents. In a previous paper, we presented pediatric dose coefficients for external photon exposures [5]. The present work, however, pertains specifically to dose coefficients for external neutron exposures; these are needed for a planned effort to update the dosimetry for the Japanese atomic bomb survivors. The Hiroshima and Nagasaki populations were exposed to a high-intensity flux of photon and neutron radiation, with ages spanning from infancy to adult [6]. Previous dose-reconstruction efforts were founded on calculations that were based on the mathematical series of phantoms introduced by Oak Ridge National Laboratory (ORNL) in the 1980s; these ORNL phantoms included the newborn; 1-, 5-, 10-, and 15-year-old; and adult reference ages. Both Yamaguchi [7] and Chou *et al* [8] previously used these ORNL phantoms to calculate neutron dose coefficients for energies up to 20 MeV. Current dosimetry for the Japanese atomic bomb survivors only categorises age within three groups: infant (based on ORNL 1-year-old phantom), child (based on ORNL 5-year-old phantom), and adult (based on ORNL 15-year-old phantom) [9].

As an improvement, this study presents new pediatric dose coefficients based on the more anatomically realistic family of hybrid phantoms developed jointly in 2010 by the University of Florida and National Cancer Institute (UF-NCI) [10]. The UF-NCI phantom family includes male and female newborn; 1-, 5-, 10-, and 15-year-old; and adult phantoms, of which the newborn to 15-year-old ages were recently adopted by the ICRP as pediatric reference phantoms. In this study, dose coefficients were calculated for six idealised, monoenergetic irradiation geometries with neutron energies ranging from 0.001 eV to 10 GeV; those up to 150 MeV will be presented. A total of 28 organs, two bone tissues, and the overall effective dose were considered. The results of this work show the dependence of neutron dose coefficients on age (a proxy for body size) and the irradiation geometry.

2. Theory and methods

2.1. Computational human phantoms

The UF-NCI hybrid phantoms used in this work were converted to voxel-formatted phantoms for radiation transport simulations using the Monte Carlo N-Particle transport code version 6.1.0 (MCNP6) (figure 1) [11]. Each phantom is composed of 53 different tissue materials defined by age-dependent elemental compositions taken from ICRP 89 and Report 46 of the International Commission on Radiation Units and Measurements (ICRU) [12, 13]. A total of 139 different tissues and organs are defined within the phantoms, of which 28 organs were tagged for dose estimation, along with trabecular bone regions within cortical bone layers.

Similar calculations were also performed for the ICRP 110 adult male and female reference voxel phantoms. Performing these calculations on the ICRP adult reference phantoms provides a convenient measure to validate our calculational methodology. As an initial step, we first verified that we could reproduce the neutron dose coefficients for the ICRP reference phantoms as published in ICRP 116; the results are described in Section 3.1.

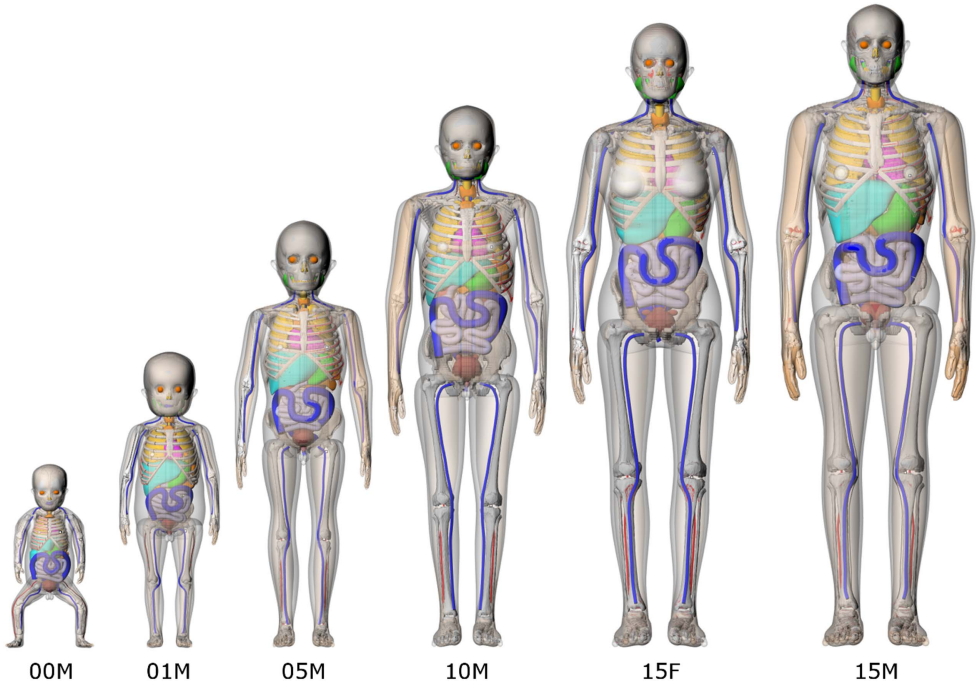

Figure 1. Frontal views of the UF-NCI pediatric reference phantom series (phantom identifier, maximum voxel dimension, height, weight): newborn male (00 M, 0.66 mm, 51 cm, 3.5 kg), 1-year-old male (01 M, 1.4 mm, 76 cm, 10 kg), 5-year-old male (05 M, 1.93 mm, 109 cm, 18 kg), 10-year-old male (10 M, 2.43 mm, 138 cm, 32 kg), and 15-year-old female (15 F, 2.83 mm, 161 cm, 53 kg) and male (15 M, 2.83 mm, 167 cm, 57 kg). For ages newborn through 10 years old, the pediatric phantom internal anatomy is identical between genders with the exception of the sex-specific organs [10].

2.2. Monte Carlo calculations

Neutron dose coefficients for the UF-NCI pediatric phantoms were calculated for the six idealised, monogenetic irradiation geometries considered in ICRP 116 (AP, PA, LLAT, RLAT, ROT, and ISO). For consistency, the dose coefficients were calculated at the same 68 neutron energies considered in ICRP 116—between 0.001 eV and 10 GeV; however, neutron cross-section library limitations in MCNP6 restricted the precision of high-energy calculations. Neutron calculations in MCNP6 require that the tissue compositions be specified in terms of both elemental and isotopic fractions. When available, cross-sections for elements composed of isotopes in their naturally occurring abundances were used (e.g. C, Mg, S, Cl, Ar, K, Ca, and Fe); otherwise, cross-sections for the most abundant isotope were considered (e.g. H, N, O, Na, P, and I). When available, nuclide cross-section data were taken from the U.S. Evaluated Nuclear Data File/B Version VI Release 6 (ENDF/B-VI.6) library, with cross-sections available for energies up to 150 MeV; most nuclides defined in the pediatric phantom models have data available within ENDF/B-VI.6. For those nuclides not included within that library, ENDF/B-VI.0 and ENDF/B-VI.1 libraries were used, with cross-section data available for energies up to 20 MeV [14]. When cross-section data at a certain energy were not available for a nuclide, MCNP6 used either the Cascade–Exciton physics model (CEM03.03, at energies below 3.5 GeV) or the Los Alamos Quark–Gluon String Model (at

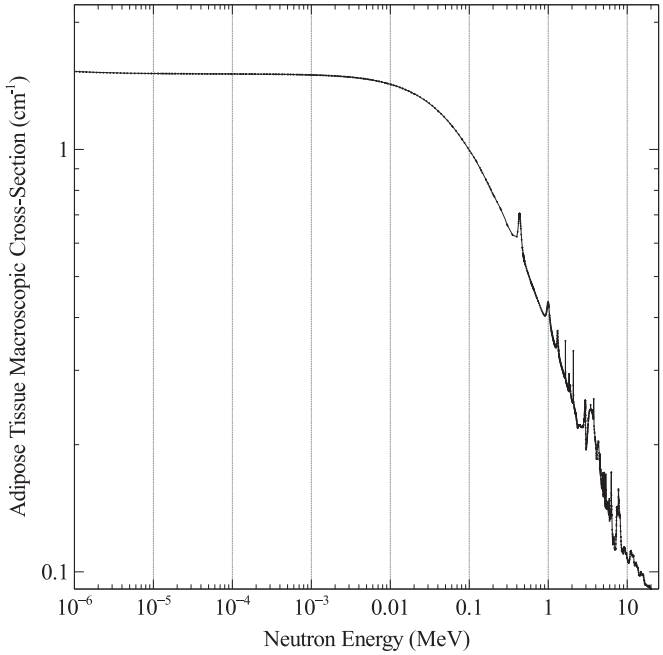

Figure 2. Macroscopic neutron cross-section versus energy for adipose tissue in the UF-NCI pediatric phantoms (1- to 15-year-old) at 293.6 K [15].

energies above 3.5 GeV) to calculate interaction cross-sections for neutrons and associated secondary particles [11]. Figure 2 shows macroscopic neutron cross-sections as a function of energy for 1- to 15-year-old phantom adipose tissue. All of the neutron cross-sections used in this study were tabulated for 293.6 K (room temperature), the closest data available to 310.15 K (normal body temperature). A special cross-section treatment for molecularly bound hydrogen in light water was applied to account for binding effects, which is important at thermal energies.

With ten pediatric phantoms, 68 neutron energies, and six different irradiation geometries, a total of 4080 MCNP model inputs were required to simulate each possible combination of parameters. This was accomplished using a Matlab (The Mathworks Inc., Natick, MA) script to automate the creation of input and voxel lattice files for each of the pediatric phantoms. Version 1.0 of MCNP6 [11] was used to calculate absorbed dose in each organ tissue of the body using the F6 tally—a kerma approximation when secondary particles are not tracked. At neutron energies below 20 MeV, the absorbed dose would be well approximated using this approach due to the limited range of secondary particles; for instance, a 20 MeV proton has a range of about 4 mm in water. Above 20 MeV, however, this approximation breaks down as secondary particle range increases beyond the thickness of certain tissues, such as shallow bone marrow and skin. For this reason, at all energies, major secondary particles—photons, protons, alpha particles, and recoil nuclei—were tracked in MCNP to account for a more detailed transport calculation; at energies above 150 MeV, pions were also tracked due to their increasing contribution to dose at these energies. Secondary electrons were not tracked in our model because of their significant contribution to dose only for neutron source energies below 1 MeV [3], where their range in tissue is less than 4 mm.

They can therefore be assumed to be depositing their energy locally, saving considerable simulation time, as electron tracking is very time-consuming in MCNP.

For each MCNP simulation, a total of 2×10^9 neutrons were sampled from an appropriate surface source irradiation geometry which covered the entire body of the phantom. All of the simulations were run on Biowulf, the National Institute of Health's high-performance Linux computing cluster. A typical compute node on the cluster consists of two central processing units (CPUs), each with eight cores, 16 threads, and a clock speed of 2.6 GHz. The simulations were expedited by allowing MCNP to assign tasks to run separately on each available thread. Under these conditions, each simulation took between 4 to 100 h to complete, with the high-energy runs consuming the most time. All 4080 MCNP simulations took approximately 1 500 000 CPU hours and were completed over the course of six weeks.

2.3. Dose conversion coefficients

Dose coefficients to 28 organs and tissues were calculated in this study for construction of effective dose: adrenal glands, brain, breasts, colon, esophagus, extrathoracic region, eye lens, gall bladder wall, heart wall, kidneys, liver, lungs, lymph nodes, muscle, oral mucosa, ovaries, pancreas, prostate, salivary glands, small intestine wall, skin, spleen, stomach wall, testes, thymus, thyroid, urinary bladder wall, and uterus.

Active marrow (red bone marrow) and shallow bone marrow (bone surface) doses were also calculated. Though we recognise the existence and practicality of using neutron skeletal fluence-to-dose conversion factors [16], the F6 tally was also used for active and shallow bone marrow dose estimation for conformity with ICRP 116 methodology. Tallies were scored at multiple bone sites, including the cervical, thoracic, and lumbar vertebrae; humeri, femora, ulnae, radii, tibiae, and fibulae; patellae spongiosa and medullary cavities; and cranium, wrists, hands, clavicles, ankles, feet, pelvis, mandible, ribs, scapulae, sacrum, and sternum. Age-dependent bone marrow distribution percentages in these sites were used to make a weighted-sum estimate of active and shallow bone marrow dose.

Python scripts were written to convert the MCNP6 tally results into organ and effective dose coefficients using the following equation:

$$\text{Dose Coefficient (pGy cm}^2) = F6\left(\frac{\text{MeV/g}}{\text{neutron emitted}}\right) \times A\ (\text{cm}^2) \times 1.602 \times 10^{-13}\left(\frac{J}{\text{MeV}}\right) \times 10^3\left(\frac{\text{g}}{\text{kg}}\right) \times 10^{12}\left(\frac{\text{pGy}}{\text{Gy}}\right), \quad (1)$$

where *F6* is the result of the MCNP tally (reported in MeV g^{-1} per neutron emitted) and *A* is the area of the neutron surface source (cm^2) used to define the irradiating field. Effective dose coefficients were calculated using the ICRP 103 radiation and tissue-weighting factors [4], with gender averaging between organs when appropriate.

3. Results and discussion

Organ dose coefficients for 28 individual organs and two bone tissues in units of dose per neutron fluence (pGy cm^2) and effective dose coefficients (pSv cm^2) were tabulated for all pediatric phantoms, as well as the ICRP adult phantoms, for 68 neutron energies ranging from 0.001 eV to 10 GeV; those up to 150 MeV are presented. Results for the ICRP adult phantoms are first compared against values found in ICRP Publication 116 to validate our calculational methodology. Subsequently, organ dose coefficients for the pediatric phantoms are plotted to

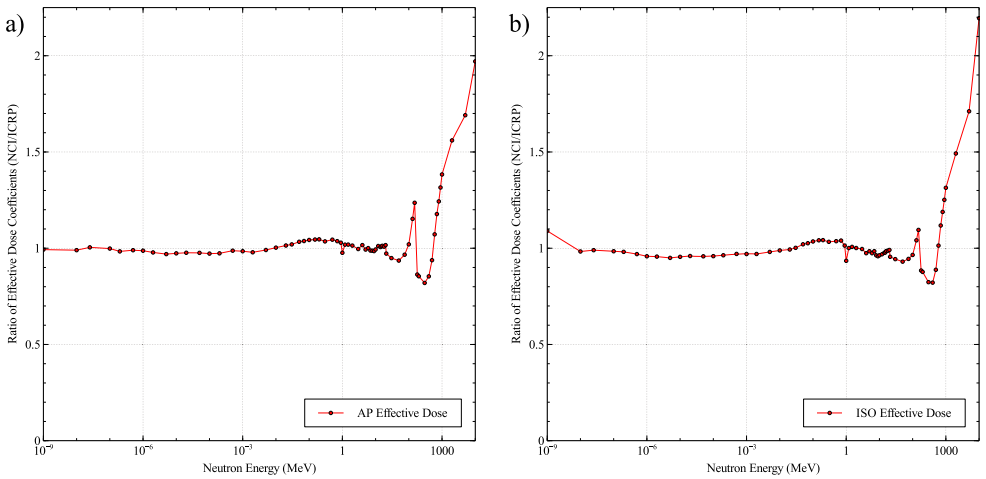

Figure 3. Ratios of the National Cancer Institute (NCI) calculations of adult dose coefficients to reference ICRP 116 values for (a) AP effective dose and (b) ISO effective dose.

show trends in dose versus age, as well as dose versus irradiation geometry. Interpolation between values, as seen in the following graphs, are performed in a linear manner. A complete data set for all organ dose coefficients, including those above 150 MeV, can be obtained within the supplementary data table available online at stacks.iop.org/JRP/38/587/mmedia. For the roughly 100 000 MCNP tallies calculated in this study, nearly all have an associated Monte Carlo statistical error below 1%, with the primary exception being in eye lens dose estimation to within 3%.

3.1. Adult phantom dose coefficients: validation of methodology

Figures 3(a) and (b) show a comparison of the neutron dose coefficients for effective dose (AP and ISO geometry, respectively) calculated in this work for the ICRP adult reference phantom with those that are published in ICRP 116. Looking at energies below 150 MeV, strong agreement is shown between the values from this study's methodology and those in ICRP 116, with values predominantly agreeing to within 10% or better. However, for values above this energy threshold, where neutron cross-section data are no longer available within MCNP for any nuclide, differences of up to 120% are seen between the two datasets. These discrepancies are attributable to the variation in physics models utilised by different simulation codes to obtain nuclear reaction cross-sections; ICRP 116 utilised multiple codes (PHITS, FLUKA, GEANT4, and MCNPX) and an averaging of the results for their dataset [3]. The ICRP neutron dose coefficient curve was also smoothed out after averaging. In our calculations, only MCNP6 was utilised, which uses the physics models described earlier. As shown previously by Sato *et al* [17], MCNPX, an earlier version of MCNP, estimates much higher dose at these energies in comparison to other codes used in ICRP 116; this may be partially from MCNP's inherent assumption that knock-on electrons produced by heavy charged particles are deposited locally. At high energies, this assumption in the MCNP model may ignore knock-on electrons with enough energy to leave the region of interaction.

In consideration of the fact that no single physics model can be confidently described as exact for these calculations, neutron dose coefficients above 150 MeV are not presented for

the pediatric phantoms; dose coefficients between 150 MeV and 10 GeV may be found in the supplementary data table for future reference to those who wish to compare estimated dose between models. These observed differences between codes in high-energy neutron dose coefficient calculation underscore the caution that should be taken when selecting a physics model.

3.2. Pediatric neutron dose coefficients

3.2.1. Effective dose tabulation. Effective dose coefficients for the UF-NCI pediatric phantoms are tabulated in table 1 for the six irradiation geometries. Up to 20 MeV, the effective dose coefficients show a nearly monotonic increase with increasing neutron energy for all phantoms with the exception of newborns; in table 1(a), newborns show a dip in effective dose from AP geometry between the energies of 10 eV to 10 keV. For all phantoms, the effective dose coefficients increase rapidly between 10 keV and 1 MeV. This is due to the swift increase in constituent organ dose and in ICRP 103 radiation weighting factors for neutrons between these energies.

3.2.2. Age dependence of dose coefficients. Figure 4 compares the dose coefficients for the different-aged phantoms for the case of dose to the female breasts (ROT irradiation geometry) and male skin (ISO geometry), which are illustrative examples of the general age-dependent trends in dose seen for other organ tissues within these phantoms. At energies roughly below 100 keV, the breast and skin dose coefficients increase with phantom age. At these energies, the major contribution to dose is from secondary photons from the hydrogen capture of thermal neutrons, producing a 2.2 MeV prompt gamma ray. Therefore, the observed trend is likely attributable to older phantoms having a larger tissue volume for neutrons to thermalise within the body and create highly penetrating secondary photons. This trend reverses at energies roughly above 100 keV, for which the dose is dominated by contributions from recoil protons resulting from the elastic scattering of hydrogen nuclei. Since dose at these energies mostly consists of energy released through elastic scattering, shielding of the organs from source neutrons becomes more important; considering how newborns lack the most shielding, this dose trend is sensible.

Figure 5 shows effective dose values for the pediatric phantoms in the AP and ISO geometries, plotted by age group. For both geometries, we again see the same general trends of dose versus age. The AP geometry shows a greater difference between ages at low energies compared to ISO, whereas the ISO geometry shows a greater difference between ages at higher energies compared to AP. This latter trend may be attributable to the greater ISO shielding difference (height and weight) between ages, since only a small amount of AP shielding change (chest wall thickness) occurs with increasing age.

Notable within figures 4 and 5 are newborn deviances from the normal trend—we see a greater dip in dose within the energy range of 10^{-6} to 10^{-2} MeV than we see with all other ages. Though multiple atypical factors come into play for the newborn phantom, one of importance is the large change in tissue elemental composition between the newborn and all other phantoms. Chou *et al* [8] implied that the unusual shape of the curve might be the result of the newborn's unique tissue element composition, whose adipose tissue contains roughly twice as much oxygen and twice as little carbon as the other pediatric phantoms. A tissue sensitivity test was performed to confirm this interpretation, where the MCNP material card of the 1-year-old was put into the input deck of the newborn. From tables 1(a) and (b), we see that the difference between newborn and 1-year-old phantoms for effective dose in ISO geometry is around 20% in the region of greatest difference (10^{-4}–10^{-3} MeV). For the

Table 1. Effective dose coefficients (pSv cm^2) for (a) newborn, (b) 1-year-old, (c) 5-year-old, (d) 10-year-old, and (e) 15-year-old phantoms exposed to external neutron fields in the AP, PA, RLAT, LLAT, ROT, and ISO irradiation geometries.

(a) Newborn	Effective Dose Coefficient (pSv cm^2)					
Energy (MeV)	AP	PA	RLAT	LLAT	ROT	ISO
1.00E-09	2.495	1.905	1.086	1.166	1.757	1.444
1.00E-08	2.794	2.190	1.154	1.248	1.935	1.544
2.50E-08	3.155	2.549	1.315	1.422	2.205	1.741
1.00E-07	3.965	3.363	1.697	1.850	2.831	2.208
2.00E-07	4.324	3.748	1.888	2.054	3.124	2.431
5.00E-07	4.751	4.220	2.143	2.333	3.491	2.710
1.00E-06	4.935	4.437	2.266	2.464	3.664	2.837
2.00E-06	5.045	4.580	2.346	2.555	3.772	2.916
5.00E-06	5.067	4.652	2.390	2.597	3.819	2.950
1.00E-05	5.045	4.664	2.404	2.601	3.814	2.948
2.00E-05	4.958	4.604	2.374	2.574	3.758	2.905
5.00E-05	4.796	4.485	2.318	2.503	3.664	2.828
0.0001	4.662	4.369	2.263	2.443	3.561	2.759
0.0002	4.518	4.251	2.211	2.380	3.459	2.676
0.0005	4.338	4.096	2.132	2.290	3.333	2.579
0.001	4.226	3.981	2.078	2.231	3.246	2.515
0.002	4.174	3.912	2.057	2.199	3.197	2.479
0.005	4.390	4.034	2.148	2.292	3.333	2.593
0.01	5.181	4.601	2.502	2.655	3.873	3.021
0.02	7.411	6.199	3.498	3.694	5.403	4.247
0.03	10.13	8.081	4.690	4.959	7.232	5.705
0.05	16.47	12.29	7.463	7.889	11.46	9.120
0.07	23.62	16.95	10.59	11.21	16.22	12.94
0.1	35.32	24.52	15.75	16.71	24.06	19.27
0.15	56.28	38.37	25.22	26.91	38.25	30.75
0.2	78.04	53.25	35.49	37.98	53.38	42.99
0.3	121.3	84.04	56.85	61.21	84.36	68.05
0.5	205.4	150.6	102.5	111.1	148.4	119.4
0.7	272.9	208.6	146.4	158.1	204.2	165.8
0.9	331.3	257.1	183.0	197.1	251.4	204.8
1	353.1	259.9	183.2	198.0	259.9	211.4
1.2	389.6	313.0	228.9	245.4	305.2	250.6
1.5	424.3	353.5	265.2	282.5	342.7	283.9
2	461.8	397.5	307.4	324.9	384.1	322.4
3	492.5	441.2	356.5	373.2	426.5	365.7
4	523.8	473.8	383.7	400.5	456.8	392.5
5	512.6	473.2	399.3	413.7	459.1	403.3
6	511.3	472.4	401.1	415.1	459.6	405.1
7	500.1	470.2	408.0	419.9	457.3	408.6
8	495.1	467.5	406.4	417.9	454.1	407.2
9	495.2	466.8	407.8	419.1	454.5	408.0
10	500.9	473.0	414.6	426.1	460.9	414.6
12	502.6	476.8	418.2	429.3	463.8	417.7
14	489.5	468.9	416.0	425.7	456.3	414.6
15	485.9	467.4	414.8	424.0	454.4	413.1
16	487.2	469.8	419.3	428.2	457.1	417.4

Table 1. (Continued.)

18	476.8	463.2	416.5	424.3	450.6	414.1
20	480.3	467.8	422.4	429.9	455.5	419.9
21	440.9	432.8	392.9	398.9	422.0	390.2
30	408.4	404.4	374.6	378.4	395.4	372.4
50	383.9	384.0	364.9	367.6	377.6	363.5
75	382.2	390.8	375.8	377.6	383.8	374.0
100	381.3	396.6	384.6	384.1	388.7	383.2
130	399.4	421.5	413.9	411.7	415.4	410.8
150	410.4	435.5	430.3	427.2	428.8	427.1
(b) 1-year-old	Effective Dose Coefficient (pSv cm^2)					
Energy (MeV)						
1.00E-09	2.407	1.811	1.214	1.272	1.759	1.427
1.00E-08	2.729	2.079	1.316	1.392	1.947	1.544
2.50E-08	3.106	2.429	1.508	1.602	2.235	1.754
1.00E-07	3.965	3.252	1.980	2.106	2.916	2.253
2.00E-07	4.388	3.664	2.212	2.365	3.255	2.503
5.00E-07	4.947	4.234	2.541	2.720	3.723	2.850
1.00E-06	5.235	4.541	2.719	2.911	3.966	3.032
2.00E-06	5.445	4.767	2.854	3.058	4.140	3.167
5.00E-06	5.609	4.962	2.961	3.176	4.294	3.276
1.00E-05	5.693	5.057	3.013	3.232	4.364	3.343
2.00E-05	5.685	5.092	3.024	3.250	4.374	3.345
5.00E-05	5.642	5.081	3.018	3.242	4.358	3.336
0.0001	5.587	5.045	2.990	3.218	4.325	3.309
0.0002	5.522	5.003	2.965	3.184	4.272	3.276
0.0005	5.428	4.936	2.915	3.134	4.212	3.227
0.001	5.362	4.886	2.885	3.103	4.168	3.195
0.002	5.375	4.878	2.892	3.102	4.167	3.194
0.005	5.686	5.082	3.033	3.253	4.379	3.362
0.01	6.634	5.767	3.494	3.745	5.049	3.885
0.02	9.163	7.569	4.732	5.045	6.827	5.266
0.03	12.09	9.557	6.146	6.507	8.840	6.875
0.05	18.48	13.64	9.189	9.682	13.20	10.32
0.07	25.25	17.70	12.41	12.99	17.72	13.93
0.1	35.74	23.76	17.37	18.10	24.65	19.52
0.15	53.48	33.85	25.90	26.80	36.43	29.01
0.2	71.34	44.22	34.68	35.78	48.46	38.67
0.3	106.1	65.30	52.19	53.74	72.25	57.74
0.5	172.8	110.6	88.13	91.14	120.3	95.91
0.7	230.6	155.3	123.0	127.7	165.0	131.7
0.9	281.3	194.5	153.7	159.8	204.2	163.0
1	298.8	198.6	157.4	163.7	213.1	170.5
1.2	335.0	242.7	192.0	200.0	250.6	200.6
1.5	371.1	281.8	223.7	233.1	285.5	229.8
2	412.4	328.1	263.2	273.7	327.8	266.1
3	455.2	385.0	315.4	326.4	378.9	313.0
4	487.7	413.4	340.6	351.4	407.5	337.5
5	488.7	434.2	365.6	376.3	423.9	358.4
6	489.2	436.8	370.7	381.5	427.5	363.4
7	483.8	443.8	382.5	392.2	432.5	372.2

Table 1. (Continued.)

8	481.2	440.0	378.5	387.1	428.7	369.1
9	480.3	440.3	382.5	391.3	430.1	372.3
10	485.7	449.8	390.8	400.0	438.2	380.5
12	489.9	455.5	396.4	405.3	443.2	385.5
14	481.2	452.8	398.3	406.4	440.7	386.8
15	479.2	453.3	398.6	406.3	440.3	386.9
16	480.8	456.5	402.5	410.0	443.2	390.9
18	472.3	451.8	401.3	407.9	438.7	389.7
20	470.0	453.1	403.2	409.7	439.3	391.7
21	439.5	427.8	382.0	387.9	413.4	370.8
30	410.2	403.6	368.7	372.6	392.0	358.6
50	388.3	387.6	364.4	366.8	379.9	355.7
75	388.5	396.7	376.7	378.7	386.2	370.6
100	392.4	404.0	387.2	389.3	394.1	381.4
130	417.0	436.9	422.5	423.3	425.8	415.9
150	431.6	456.7	443.8	443.3	445.1	439.8

(c) 5-year-old Energy (MeV)	Effective Dose Coefficient (pSv cm^2)					
1.00E-09	2.779	1.886	1.081	1.174	1.853	1.483
1.00E-08	3.223	2.176	1.155	1.267	2.083	1.619
2.50E-08	3.709	2.542	1.316	1.452	2.391	1.841
1.00E-07	4.790	3.407	1.706	1.891	3.112	2.373
2.00E-07	5.298	3.852	1.895	2.109	3.464	2.631
5.00E-07	5.927	4.457	2.159	2.396	3.932	2.973
1.00E-06	6.245	4.781	2.294	2.550	4.173	3.156
2.00E-06	6.469	5.028	2.390	2.660	4.350	3.280
5.00E-06	6.627	5.243	2.466	2.746	4.488	3.379
1.00E-05	6.688	5.357	2.501	2.782	4.558	3.434
2.00E-05	6.670	5.403	2.504	2.794	4.557	3.439
5.00E-05	6.596	5.403	2.491	2.769	4.532	3.419
0.0001	6.511	5.379	2.466	2.748	4.489	3.389
0.0002	6.413	5.345	2.439	2.716	4.444	3.353
0.0005	6.283	5.286	2.398	2.672	4.377	3.299
0.001	6.214	5.244	2.370	2.642	4.321	3.264
0.002	6.205	5.244	2.367	2.638	4.329	3.261
0.005	6.560	5.483	2.487	2.766	4.545	3.436
0.01	7.625	6.229	2.861	3.187	5.235	3.961
0.02	10.49	8.165	3.876	4.307	7.059	5.365
0.03	13.81	10.29	5.030	5.581	9.139	6.972
0.05	21.12	14.58	7.568	8.382	13.62	10.44
0.07	28.93	18.80	10.27	11.34	18.29	14.08
0.1	41.12	24.97	14.51	15.98	25.46	19.73
0.15	61.91	34.99	21.83	24.03	37.62	29.38
0.2	82.73	45.02	29.42	32.32	49.91	39.13
0.3	122.9	64.85	44.51	48.94	74.00	58.32
0.5	198.8	106.9	74.85	82.55	121.6	96.10
0.7	261.1	148.1	103.5	114.3	164.4	130.5
0.9	314.9	183.9	128.5	142.0	201.5	160.4
1	332.2	185.4	131.7	146.1	209.4	166.7
1.2	370.1	228.5	159.1	175.7	244.6	195.6

Table 1. (Continued.)

1.5	405.6	265.5	185.3	203.7	277.5	223.1
2	445.4	310.6	218.9	239.1	316.9	257.0
3	483.6	367.4	266.5	287.4	365.7	301.0
4	518.1	396.8	288.7	310.7	394.6	325.3
5	511.8	417.8	316.0	336.3	409.9	344.5
6	512.9	423.2	322.9	343.0	415.4	350.8
7	503.7	431.7	338.2	356.3	420.6	359.4
8	501.8	427.4	337.1	354.0	418.1	358.1
9	500.5	429.8	341.0	357.9	420.0	361.0
10	504.4	438.9	349.2	366.5	427.5	368.4
12	509.2	446.5	355.8	372.6	433.8	374.4
14	498.9	445.6	361.0	376.3	432.3	376.5
15	496.5	447.1	362.2	377.0	432.6	377.1
16	496.8	449.4	367.2	381.4	435.3	380.8
18	487.0	445.9	368.8	381.5	431.8	380.3
20	484.0	447.5	372.1	384.5	432.9	382.8
21	453.5	424.4	354.8	365.8	408.9	363.4
30	419.7	402.5	348.6	356.4	389.3	353.6
50	395.8	389.0	353.0	357.3	379.5	353.7
75	395.3	398.2	370.3	374.4	387.0	368.4
100	396.3	407.9	385.2	387.2	395.2	381.0
130	419.5	442.5	422.0	422.9	427.8	416.1
150	434.1	465.7	446.7	446.8	450.2	439.8

(d) 10-year-old Energy (MeV)	Effective Dose Coefficient (pSv cm^2)					
1.00E-09	2.598	1.733	1.080	1.149	1.751	1.398
1.00E-08	2.991	1.981	1.164	1.251	1.955	1.524
2.50E-08	3.441	2.308	1.331	1.431	2.250	1.734
1.00E-07	4.458	3.075	1.722	1.859	2.930	2.236
2.00E-07	4.945	3.471	1.922	2.075	3.260	2.478
5.00E-07	5.590	4.031	2.192	2.364	3.719	2.821
1.00E-06	5.933	4.345	2.336	2.527	3.968	2.999
2.00E-06	6.185	4.589	2.446	2.646	4.162	3.140
5.00E-06	6.388	4.819	2.543	2.751	4.325	3.261
1.00E-05	6.503	4.951	2.589	2.803	4.412	3.320
2.00E-05	6.530	5.020	2.614	2.824	4.446	3.350
5.00E-05	6.513	5.062	2.609	2.831	4.446	3.354
0.0001	6.469	5.074	2.602	2.823	4.435	3.344
0.0002	6.414	5.075	2.592	2.808	4.419	3.328
0.0005	6.349	5.062	2.570	2.786	4.384	3.306
0.001	6.311	5.056	2.556	2.773	4.373	3.297
0.002	6.338	5.091	2.569	2.788	4.399	3.319
0.005	6.715	5.369	2.716	2.944	4.648	3.514
0.01	7.782	6.132	3.133	3.403	5.355	4.065
0.02	10.60	8.060	4.237	4.579	7.222	5.495
0.03	13.80	10.13	5.475	5.917	9.304	7.110
0.05	20.66	14.28	8.129	8.755	13.69	10.54
0.07	27.80	18.24	10.87	11.70	18.15	14.07
0.1	38.67	23.84	15.09	16.17	24.85	19.43
0.15	56.72	32.47	22.10	23.65	35.84	28.24

Table 1. (Continued.)

0.2	74.37	40.63	29.14	31.07	46.63	36.92
0.3	107.9	55.89	42.60	45.43	67.04	53.45
0.5	170.7	86.82	68.78	73.49	106.2	84.87
0.7	224.0	118.2	93.26	99.91	142.0	113.4
0.9	269.7	145.3	114.4	122.7	172.8	138.0
1	280.6	143.0	115.7	123.9	176.8	141.9
1.2	318.8	180.4	140.6	151.0	209.1	167.3
1.5	353.7	212.9	164.2	176.2	239.0	191.5
2	394.5	254.2	195.4	209.0	276.5	222.5
3	440.0	312.4	242.3	257.2	326.6	265.8
4	473.2	339.3	263.5	278.9	354.0	288.1
5	477.9	369.6	294.2	309.3	376.3	311.2
6	482.8	378.9	303.6	318.3	384.6	319.7
7	479.9	393.9	321.8	335.4	394.9	332.0
8	478.6	390.8	320.0	333.0	393.1	330.6
9	478.3	394.9	325.9	338.6	396.4	335.0
10	483.4	404.9	334.5	347.5	404.6	342.9
12	490.3	414.4	342.7	355.3	412.5	350.2
14	484.2	418.7	350.9	362.5	415.1	355.5
15	483.6	421.7	353.3	364.6	416.7	357.2
16	483.9	424.7	358.1	368.9	419.6	360.9
18	476.3	424.0	361.1	371.1	418.2	362.2
20	473.2	426.3	364.2	374.0	419.4	364.8
21	448.1	409.4	351.3	359.8	401.2	350.4
30	418.6	395.2	349.4	355.9	386.9	345.3
50	397.8	387.0	356.4	360.4	379.7	349.4
75	399.0	398.8	374.3	377.0	390.5	367.0
100	403.1	410.5	388.6	390.2	401.5	381.5
130	432.0	451.7	428.2	429.4	437.8	420.2
150	451.6	479.1	455.9	455.9	462.7	447.0
(e) 15-year-old Energy (MeV)	Effective Dose Coefficient (pSv cm^2)					
1.00E-09	2.694	1.665	0.9575	1.070	1.705	1.370
1.00E-08	3.145	1.910	1.022	1.157	1.920	1.505
2.50E-08	3.658	2.232	1.165	1.327	2.216	1.720
1.00E-07	4.808	2.985	1.516	1.735	2.904	2.236
2.00E-07	5.365	3.380	1.695	1.941	3.251	2.493
5.00E-07	6.102	3.936	1.939	2.223	3.721	2.845
1.00E-06	6.488	4.250	2.075	2.376	3.976	3.037
2.00E-06	6.774	4.497	2.173	2.489	4.171	3.180
5.00E-06	7.008	4.732	2.258	2.588	4.339	3.308
1.00E-05	7.133	4.866	2.303	2.639	4.429	3.374
2.00E-05	7.163	4.940	2.318	2.657	4.469	3.402
5.00E-05	7.145	4.996	2.322	2.658	4.476	3.410
0.0001	7.104	5.013	2.315	2.650	4.468	3.405
0.0002	7.053	5.020	2.303	2.632	4.447	3.390
0.0005	6.971	5.019	2.281	2.610	4.417	3.366
0.001	6.928	5.025	2.270	2.592	4.399	3.353
0.002	6.948	5.066	2.276	2.601	4.422	3.367
0.005	7.329	5.354	2.397	2.738	4.661	3.555

Table 1. (Continued.)

0.01	8.446	6.119	2.750	3.141	5.355	4.080
0.02	11.34	8.048	3.675	4.198	7.139	5.449
0.03	14.60	10.12	4.708	5.380	9.116	6.963
0.05	21.54	14.24	6.890	7.875	13.23	10.13
0.07	28.63	18.14	9.141	10.44	17.37	13.35
0.1	39.38	23.58	12.55	14.34	23.51	18.17
0.15	57.23	31.76	18.29	20.90	33.56	26.04
0.2	74.86	39.31	24.06	27.52	43.39	33.85
0.3	108.4	52.98	35.27	40.45	61.99	48.71
0.5	172.6	79.87	57.45	66.20	98.13	77.60
0.7	227.0	107.0	78.34	90.42	131.1	104.2
0.9	273.1	130.2	96.12	111.0	159.2	126.9
1	280.9	125.8	96.93	112.3	161.1	128.7
1.2	323.0	161.2	118.3	136.6	192.8	154.1
1.5	359.3	191.6	138.2	159.0	221.1	177.2
2	401.0	231.2	164.8	188.1	256.8	206.9
3	447.6	289.9	206.3	231.8	306.1	249.3
4	481.1	316.2	224.9	251.8	331.9	270.5
5	485.5	350.1	254.6	280.8	356.1	294.4
6	491.4	361.7	264.5	290.3	366.0	303.9
7	488.1	379.7	283.8	308.0	377.8	317.3
8	486.9	376.4	283.1	306.7	376.2	316.2
9	486.4	382.0	289.1	312.2	380.4	321.0
10	491.3	392.7	297.7	320.9	388.7	328.8
12	498.7	403.8	306.3	329.1	397.7	336.8
14	492.7	410.6	316.8	337.8	402.2	343.5
15	492.3	414.9	319.8	340.3	404.5	345.8
16	491.9	417.7	325.0	345.0	407.4	349.6
18	483.9	418.8	330.3	348.6	407.3	352.1
20	480.4	421.3	334.5	352.4	408.9	354.8
21	456.4	407.6	325.0	340.9	393.5	342.7
30	425.7	396.3	329.9	341.7	382.8	340.8
50	403.5	389.8	344.1	351.7	378.8	347.9
75	406.2	401.4	367.5	372.3	391.9	368.6
100	410.6	414.7	384.9	388.6	403.4	383.3
130	439.8	457.3	426.5	429.2	441.8	423.1
150	459.6	487.4	455.9	457.6	468.4	451.2

material-tested newborn, a 0.6% effective dose increase was seen at 10^{-3} MeV due to the change in tissue element composition. This small increase is not enough to suggest that it is the major cause of the observed differences; geometry of the phantoms appears to be the most important factor.

3.2.3. Field geometry dependence of dose coefficients. In figure 6, active marrow and stomach wall organ dose coefficients are plotted in all six irradiation geometries for the 10-year-old female and male, respectively. For the active bone marrow (figure 6(a)), we see that a PA exposure results in the largest dose at all energies, which can be attributed to the large portion of red marrow in the lumbar and thoracic spine near the back of the body. It is also worth pointing out the similarity in LLAT and RLAT values at all energies, which should

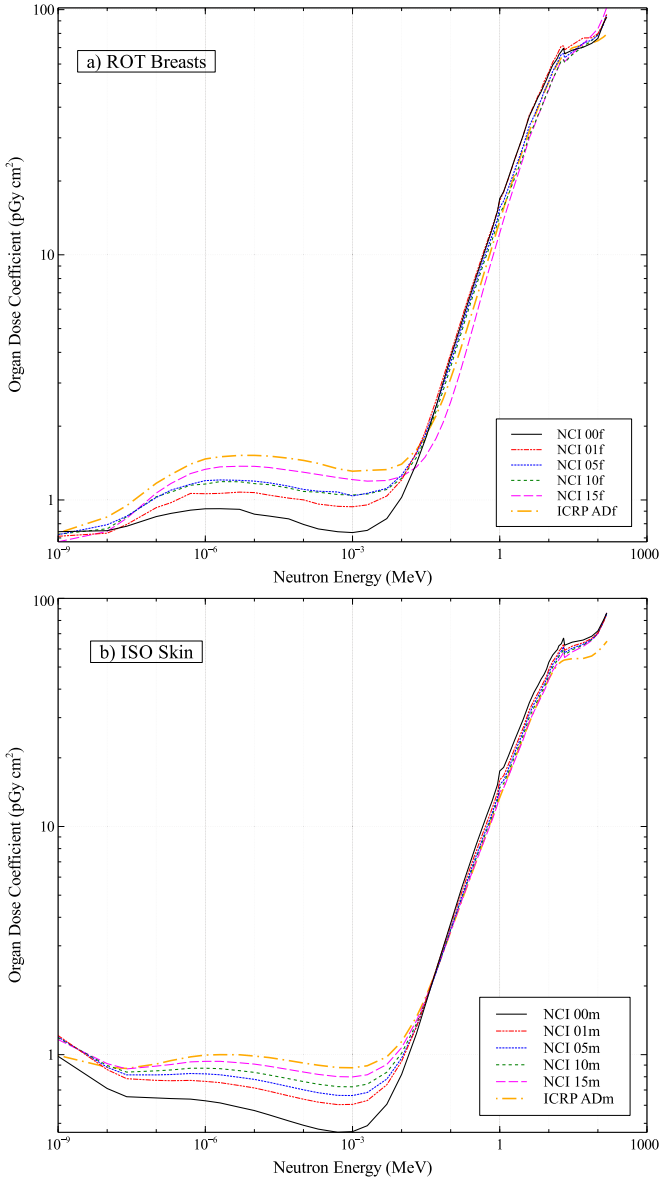

Figure 4. Neutron dose coefficients for breasts and skin as a function of age (newborn—adult) for the (a) ROT and (b) ISO geometries, respectively.

occur for a symmetrical skeleton. In figure 6(b), we see that the stomach wall receives the largest dose for AP exposure, likely due to its position near the front and the comparatively large projected area of the AP field on the organ. As expected, the dose for LLAT exposure is also significantly greater than for a RLAT exposure at these energies; this is attributable to the position of the stomach on the left side of the body, which provides shielding against neutrons incident on the body from the RLAT direction.

An unusual feature observed on many of the organ dose coefficient plots was a bend at 1 MeV—bumps can be seen in the age comparison of figure 4, and dips can be seen in the

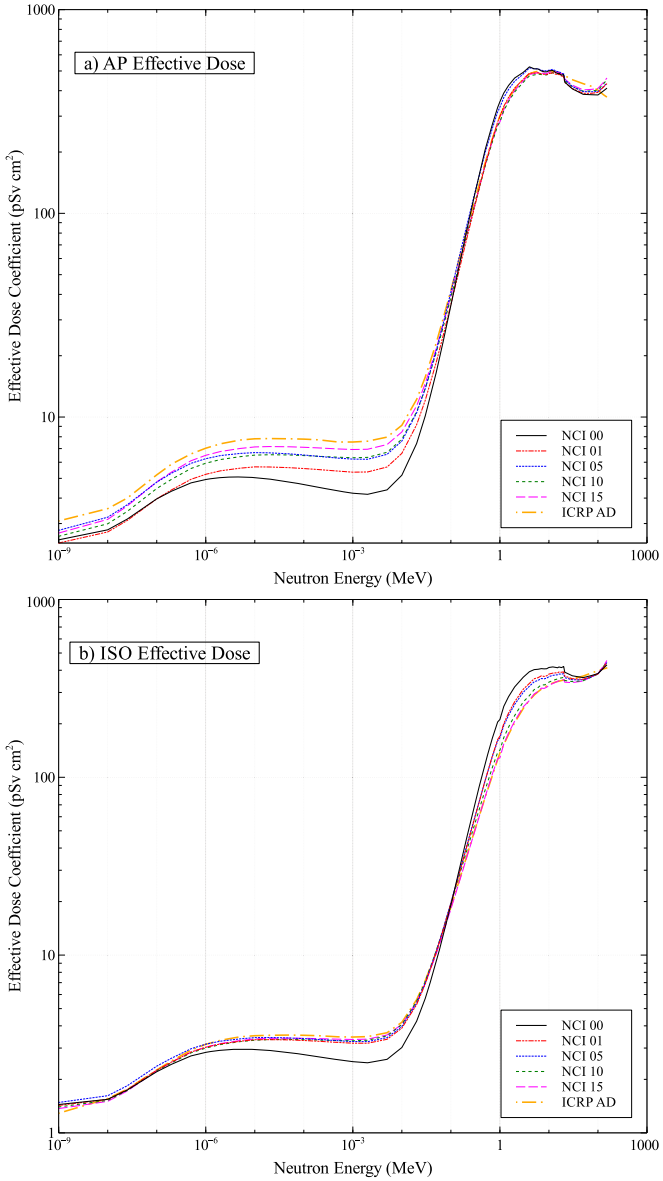

Figure 5. Neutron effective dose coefficients as a function of age (newborn—adult) for the (a) AP and (b) ISO geometries.

geometry comparison of figure 6. We hypothesised that this is the result of a spike in neutron total cross-section for adipose tissue at this energy, as seen in figure 2. With data points for dose coefficients captured at 0.9, 1.0, and 1.2 MeV, the peak in cross-section is well captured within our data; this is unlike the peak in cross-section at 0.4 MeV, which the data grid overlooks with simulations only at 0.3 and 0.5 MeV. Quick tests performed by dose coefficient calculation at 0.4 MeV showed that similar plot deformities were introduced into the curve when including the new data point.

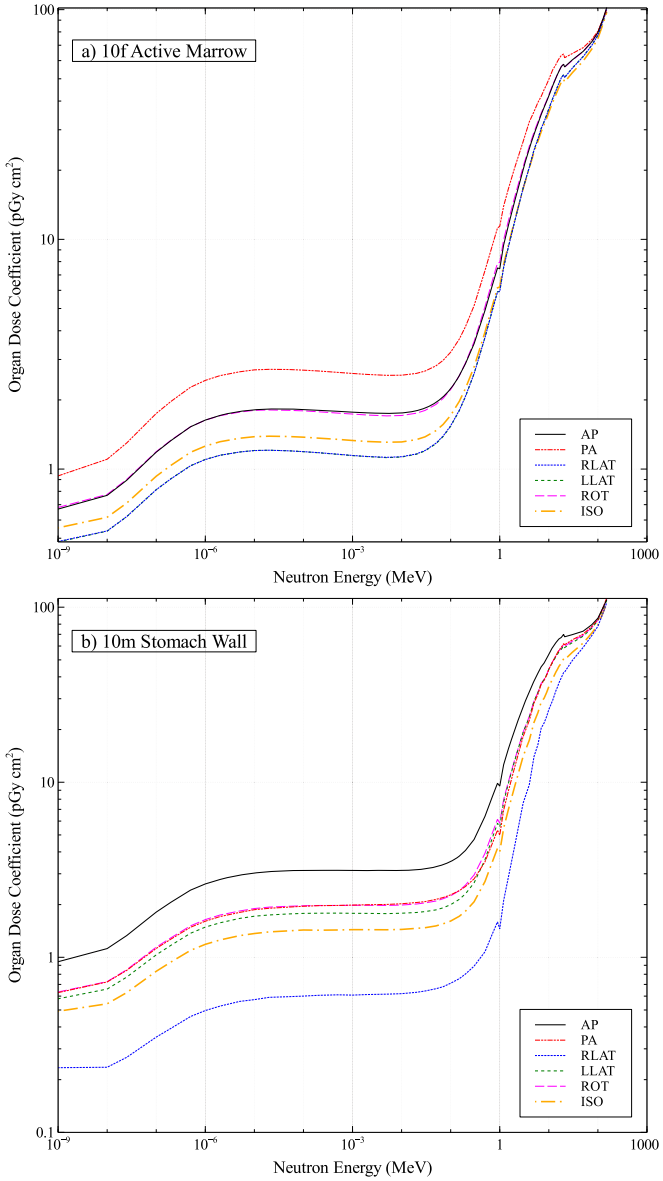

Figure 6. Neutron dose coefficients in the six irradiation geometries for (a) active marrow and (b) stomach wall organs for the 10 f and 10 m phantoms, respectively.

In figure 7, effective dose for the 1-year-old phantom is plotted for all six irradiation geometries. Similar trends in the effective dose coefficients were observed for all phantom ages. At all energies, the AP geometry experiences the greatest amount of dose; this occurs because most organs with the highest tissue-weighting factors are located closer to the front of the body. The effective dose coefficients for the LLAT exposure are greater than for the RLAT irradiation geometry, which is mostly attributable to the highly weighted stomach wall, as discussed before with figure 6.

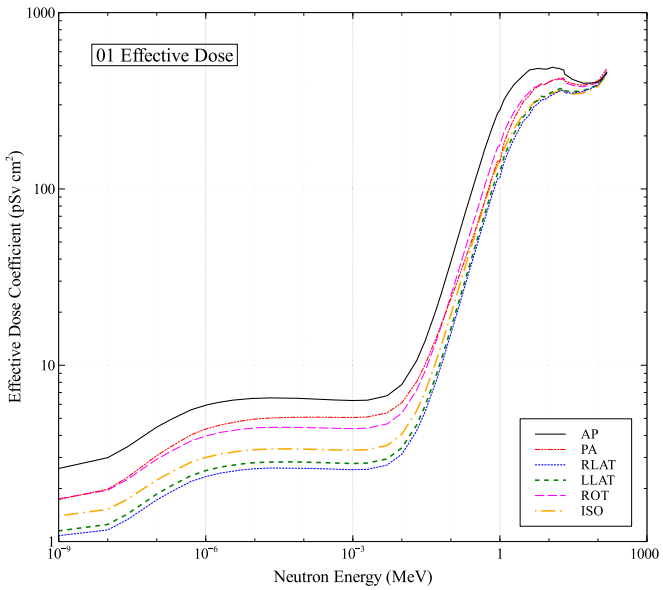

Figure 7. Neutron effective dose coefficients for the 1-year-old phantom in each of the six irradiation geometries. This plot trend for effective dose is seen for every-aged phantom in the UF-NCI series.

3.3. Limitations

Within our methodology, the foremost constraint was in cross-sectional data availability, particularly above 150 MeV. As seen in the validation results, this creates an irregular drop in dose coefficients and an eventual departure from ICRP 116 reference values at the high end of our energy grid. It is important to point out that ICRP 116 utilised multiple codes and a curve-smoothing technique to create dose coefficients. Until cross-sectional data are developed for ultrafast neutrons within Monte Carlo codes, the results we present above 150 MeV should be taken as preliminary and used with care.

Regarding application of these results, it is necessary to pay close attention to differences between real-world conditions and the idealised scenarios modeled in this study. First, the calculated results assume a whole-body neutron exposure and should not be used in the case of a partial-body exposure. Second, if the exposure geometry is unknown, the conservative choice for radiation-protection purposes is to use the largest dose coefficient for the most closely matching phantom in height and weight. As we showed in this work, the most conservative choice of dose coefficients can vary with age and neutron energy. Third, it should be pointed out that it is quite infrequent for a child or adolescent to be exposed to whole-body neutron irradiation; such scenarios often occur in occupational settings such as those within a nuclear facility or near a high-energy accelerator. One possible exposure source for children and adolescents could be the Japanese atomic bomb survivors who were children or adolescents at the time; another could be from the cosmic radiation field experienced during travel at high elevations [18]. For either case, the selection of irradiation geometry will significantly impact the resulting dose estimation, as seen in our geometry-comparison plots (figures 6 and 7); however, neither exposure scenario would be ideally described by one of the ICRP irradiation geometries. Inherent uncertainty may therefore arise from the application of an idealised irradiation field to a specific exposure scenario. Lastly, the dose coefficients

derived in this study are for the UF-NCI phantoms and correctly apply to the respective children and adolescents they are based on. Variation in body size, organ positioning, and the physical orientation of the body during exposure are all factors that will vary from case to case.

The use of effective dose in monitoring risk to children and adolescents demands that caution be taken as well. The ICRP 103 tissue and radiation weighting factors utilised in this study were not designed specifically for use with any age group; they are intended to apply as rounded values to a population of both sexes and all ages. It is therefore notable that effective dose, as calculated here, is limited in being age-dependent only through its constituent organ doses and not necessarily through the contributing weights of each organ. Future work to improve the age dependence of these regulatory quantities can be performed once age-dependent tissue and radiation weighting factors have been developed.

4. Conclusions

We have compiled a vast neutron dose coefficient dataset for the UF-NCI pediatric phantoms covering a wide range of neutron energies (0.001 eV to 10 GeV) and six different irradiation geometries. Dose coefficients were calculated for 28 individual organs, two bone tissues, and the whole-body effective dose. Results for the ICRP reference adult phantoms showed excellent agreement with those published in ICRP 116, demonstrating both the legitimacy and limitations (above 150 MeV) of our calculations. The results of the present study demonstrate how organ dose depends strongly on phantom age (a proxy for body size), neutron energy, and irradiation geometry. For a fixed irradiation geometry, the energy of the neutron source is the primary determinant as to whether a younger individual receives higher or lower organ doses compared to an adult. Below 100 keV, dose tends to increase with age whereas, above 100 keV, dose tends to decrease with age. Though exceptions in these general trends do occur, especially for newborns, they demonstrate the significant difference in organ-absorbed dose between age groups. Unsurprisingly, the geometry of the irradiation field also plays an important role.

A comprehensive table of all neutron dose coefficients found in this study, including those above 150 MeV, is accessible online in Microsoft Excel format as a supplementary data table. Our extension of neutron dose coefficient values will provide beneficial data to applications such as the Japanese atomic bomb survivor studies, as well as to pediatric studies of cosmic irradiation at high elevations.

Acknowledgments

We would like to thank Doctor Akira Endo of the Japan Atomic Energy Agency for his assistance in improving the scope of this study and the examination of its results. This work was funded by the intramural program of the National Institutes of Health, National Cancer Institute, Division of Cancer Epidemiology and Genetics. The contents are solely the responsibility of the authors and do not necessarily represent the official views of the National Institutes of Health. The calculations in this work were performed on the National Institutes of Health's High-Performance Computing Biowulf cluster (http://hpc.nih.gov).

Disclaimer

Certain commercially available software is identified in this manuscript to foster understanding. Such identification does not imply recommendation by the National Institutes of Health, nor does it necessarily imply that they are the best available for the purpose.

References

[1] Xu X G 2014 An exponential growth of computational phantom research in radiation protection, imaging, and radiotherapy: a review of the fifty-year history *Phys. Med. Biol.* **59** R233–302
[2] ICRP 2009 Adult reference computational phantoms. ICRP Publication 110 *Ann. ICRP* **39** 1–165
[3] ICRP 2010 Conversion coefficients for radiological protection quantities for external radiation exposures. ICRP Publication 116 *Ann. ICRP* **40** 1–257
[4] ICRP 2007 The 2007 recommendations of the International Commission on Radiological Protection. ICRP Publication 103 *Ann. ICRP* **37** 1–332
[5] Chang L A *et al* 2017 Dose coefficients for ICRP reference pediatric phantoms exposed to idealised external gamma fields *J. Radiol. Prot.* **37** 127–46
[6] Kerr G D 1979 Organ dose estimates for the Japanese atomic bomb survivors *Health Phys.* **37** 487–508
[7] Yamaguchi Y 1994 Age-dependant effective doses for neutron from thermal to 18.3 MeV *Radiat Prot Dosim.* **55** 257–63
[8] Chou D P *et al* 2003 Age-dependent protection quantities for external neutron irradiation *Radiat Prot Dosim.* **104** 5–16
[9] Cullings H M, Kawamura H and Chen J 2012 Body and organ dimensions of the 1945 Japanese population used in dosimetry system DS86 and data available for an expanded series of phantoms *Radiat. Prot. Dosim.* **149** 35–42
[10] Lee C *et al* 2010 The UF family of reference hybrid phantoms for computational radiation dosimetry *Phys. Med. Biol.* **55** 339–63
[11] Pelowitz D B 2013 *MCNP6 User's Manual Version 1.0* (Los Alamos National Laboratory)
[12] ICRP 2002 Basic anatomical and physiological data for use in radiological protection reference values. ICRP Publication 89 *Ann. ICRP* **32** 1–277
[13] ICRU 1992 *Photon, Electron, Proton, and Neutron Interaction Data for Body Tissues* (International Commission on Radiation Units and Measurements)
[14] Conlin J L *et al* 2014 *Listing of Available ACE Data Tables* (Los Alamos National Laboratory)
[15] Zerkin V 2017 *ENDF: Evaluated Nuclear Data File—Database Version of 2017-06-01* (International Atomic Energy Agency)
[16] Bahadori A A *et al* 2011 Response functions for computing absorbed dose to skeletal tissues from neutron irradiation *Phys. Med. Biol.* **56** 6873–97
[17] Sato T *et al* 2009 Fluence-to-dose conversion coefficients for neutrons and protons calculated using the PHITS code and ICRP/ICRU adult reference computational phantoms *Phys. Med. Biol.* **54** 1997–2014
[18] Wilson J W, Clowdsley M S, Shinn J L, Singleterry R C, Tripathi R K, Cucinotta F A, Heinbockel J H, Badavi F F and Atwell W 2000 Neutrons in space: shield models and design issues *30th Int. Conf. on Environmental Systems (Toulouse, France)*